Research Article

URF PUBLISHERS
connect with research world

Journal of Petroleum & Chemical Engineering

https://urfpublishers.com/journal/petrochemical-engineering

Vol: 4 & Iss: 2

Enhancing Oil Recovery in Heterogeneous Reservoirs with CO2 Flooding

Nurlan Alakparov*

PhD Programs, Azerbaijan State Oil and Industry University, Azerbaijan

Citation: Alakparov N. Enhancing Oil Recovery in Heterogeneous Reservoirs with CO2 Flooding. *J Petro Chem Eng* 2026;4(2):348-359.

Received: 10 April, 2026; **Accepted:** 09 June, 2026; **Published:** 12 June, 2026

***Corresponding author:** Nurlan Alakparov, PhD Programs, Azerbaijan State Oil and Industry University, Azerbaijan

ABSTRACT

This research explores the key challenges associated with CO_2-enhanced oil recovery (EOR), emphasizing the influence of fine-scale reservoir characteristics, viscous and interfacial dynamics and dispersion effects driven by concentration gradients. The focus is on understanding how these microscale parameters affect oil extraction efficiency during CO_2 injection.

A series of simulation models reflecting different heterogeneity configurations was created and tested under varying pressure conditions, both above and below the Minimum Miscibility Pressure (MMP). A basic two-dimensional reservoir model was constructed as a compositional oil simulation using Eclipse 300. The grid comprises 100 cells along the x-axis and 20 cells along the z-axis, totaling 2000 cells. To replicate injection and production processes, two vertical wells were positioned at opposite ends of the model, fully penetrating the z-direction. This setup enables CO_2 to displace oil effectively from the injection well toward the production well.

Following 21 simulation runs, the findings indicated that when operating below the Minimum Miscibility Pressure (MMP), gravitational forces dominated the displacement process, leading to gas overriding oil, while permeability had a relatively minor influence. In contrast, at pressures above the MMP, viscous forces triggered fingering and premature breakthrough. All scenarios demonstrated enhanced oil recovery due to miscibility, with the kv/kh ratio emerging as a key parameter. Increased horizontal permeability or simultaneous increases in both horizontal and vertical permeabilities, negatively affected recovery performance. Gas override was governed by both permeability directions, contributing to fingering in cases with randomly distributed permeability. Variations in horizontal permeability, even when vertical permeability remained constant, had the most pronounced effect on recovery efficiency. Moreover, the study highlighted that relying solely on the coefficient of variation (Cv) was insufficient to describe heterogeneity, as models sharing identical Cv values yielded recovery rates ranging from 62% to 95.9%.

The unique contribution of this study lies in its quantitative assessment of how reservoir heterogeneity influences CO_2-enhanced oil recovery (EOR). The results highlight the complex interplay between reservoir characteristics and CO_2 miscible flooding, providing valuable guidance for refining EOR approaches in heterogeneous formations.

Keywords: CO_2-enhanced oil recovery; Vertical permeability; Horizontal Permeability; Minimum Miscibility Pressure (MMP); Heterogeneous Reservoirs

Introduction

In recent decades, global oil production has surged in response to rising energy demand worldwide[1]. To satisfy this growing need, various recovery techniques have been implemented to extract additional oil from mature and depleted reservoirs[2]. Despite the use of primary recovery methods that rely on natural reservoir energy and secondary techniques such as water flooding, a substantial volume of oil remains trapped within the fine pores of reservoir rocks. Enhanced Oil Recovery (EOR) technologies have long been employed to boost extraction efficiency and reduce residual oil saturation[1]. The primary aim of EOR is to improve the mobility ratio between injected and displaced fluids, thereby enhancing sweep efficiency or modifying interfacial tension and capillary pressure[3]. As a result, EOR continues to be recognized as a critical technological frontier in the petroleum sector[4].

Enhanced Oil Recovery (EOR) techniques are generally categorized into three main types: chemical, thermal and miscible approaches[5]. Chemical EOR methods include polymer flooding, alkaline flooding and surfactant flooding[6,7]. These techniques improve oil displacement by introducing specific chemicals into the injected water to alter fluid viscosity or modify interfacial properties, thereby achieving a more favourable mobility ratio[8]. Thermal EOR strategies involve processes such as cyclic steam stimulation, steam flooding and in-situ combustion[9]. These methods utilize heat to lower oil viscosity[10] and in some cases, vaporize lighter hydrocarbon fractions into the gas phase, making the oil less dense and easier to mobilize[11,12]. Miscible EOR techniques rely on injecting substances like Liquefied Petroleum Gas (LPG), Nitrogen or Carbon Dioxide (CO_2. Miscible displacement was defined as “the displacement of oil by fluids with which it mixes in all proportions without the presence of an interface[13]”.

CO_2 stands out as a highly effective agent in Enhanced Oil Recovery (EOR) due to its distinctive miscibility characteristics. As such, CO_2-EOR offers a dual advantage-boosting energy output while promoting environmental stewardship-making it a vital technology for optimizing resource extraction and reducing carbon emissions in the oil and gas sector[14]. In aging reservoirs, traditional recovery methods often leave a considerable amount of oil trapped within the formation[15]. The injection of supercritical CO_2 into these reservoirs mobilizes the remaining oil through several key mechanisms[16]. First, CO_2 dissolves into the oil, leading to expansion and reduced viscosity, which enhances its movement toward production wells. This process, known as “miscible displacement,” yields significantly higher recovery rates compared to water flooding. Second, CO_2 interacts with reservoir rock surfaces, modifying wettability and facilitating oil release. Additionally, CO_2-EOR provides further advantages: it serves as a long-term storage solution for captured CO_2, helping to mitigate greenhouse gas emissions and adds economic value by revitalizing depleted oilfields[17].

Deploying CO_2-EOR in mature oil reservoirs presents several challenges that can potentially compromise the feasibility of such projects[18]. These obstacles include fine-scale reservoir characteristics, viscous and interfacial forces that influence fluid dynamics and dispersion effects arising from concentration gradients between fluids[19]. A key factor affecting reservoir performance during CO_2 injection is heterogeneity, which refers to the spatial variation in rock attributes such as porosity, permeability, facies distribution and layer thickness[20]. Such heterogeneities may lead to early CO_2 breakthrough, resulting in channelling and dispersion that hinder effective oil displacement and reduce project efficiency. Addressing these issues requires thorough reservoir evaluation, the use of sophisticated simulation tools and detailed risk analysis[21]. Professionals involved in CO_2-EOR must consider how heterogeneity influences fluid movement and recovery efficiency[22]. Adjustments in injection strategies, well positioning and operational settings may be necessary to overcome these limitations. Continued innovation and research in EOR technologies are essential for enhancing the effectiveness of CO_2-EOR, especially in aging oilfields[23].

The primary objective of this research is to examine how fine-scale reservoir characteristics influence oil recovery during CO_2 injection. This includes replicating the slim tube experiments originally conducted by Holm and Josendal through high-resolution simulation models[24]. It is well established that CO_2 becomes miscible with oil in one-dimensional systems under sufficient pressure. However, actual reservoir formations are complex and exhibit heterogeneity, with fluid flow occurring in three dimensions. It remains unclear whether miscibility effects diminish or intensify under such conditions. Additionally, gravity override may cause CO_2 to bypass oil zones, limiting interaction and mixing. To identify the dominant factors affecting recovery, a range of models with varying static heterogeneity patterns has been developed. Sensitivity analyses have been performed to evaluate how reservoir heterogeneity impacts gas miscibility, oil recovery and the role of the coefficient of variation in influencing recovery outcomes.

Methodology

Base case description

To investigate the influence of fine-scale geological features on CO_2-EOR performance, a basic 3D grid model was developed using the Eclipse reservoir simulator (E-300). The model spans dimensions of 10 m × 1 m × 2 m and comprises 2000 cells, each measuring 0.1 m × 0.1 m × 0.1 m, arranged as 100 cells along the x-axis and 20 cells along the z-axis. The reference case is a compositional oil model with uniform rock properties, detailed in Table A.1 of Appendix A. Fluid characteristics, including density and formation volume factors, were initially calculated using the Peng-Robinson equation of state for a seven-component reservoir fluid system (Table A.2), while Table A.3 presents the oil-gas relative permeability curves. For simulating injection and production, two vertical wells were positioned-an injector at grid cell (1,1) and a producer at (100,1). Both wells were completed across all 20 layers to ensure vertical coverage, enabling CO_2 to displace oil from the injection point to the production well. The producer was set to operate at a minimum Bottom Hole Pressure (BHP) equal to the reservoir pressure (50 bar), which was later increased above the Minimum Miscibility Pressure (MMP). The injector was configured to deliver 1.2 pore volumes (PV) of CO_2 at a rate of 0.48 m^3/day over a 12-hour period. **(Figure 1)** illustrates the initial gas saturation distribution within the model.

Scenarios investigated

To evaluate the impact of reservoir heterogeneity, multiple scenarios were developed, each featuring distinct permeability distributions across the layers. Simulations were conducted at varying reservoir pressures ranging from 50 to 300 bars. Following this, 1.2 pore volumes (PV) of CO_2 were injected and oil recovery was plotted against pressure to identify the Minimum Miscibility Pressure (MMP). Additionally, gas saturation patterns were analysed at pressures both above and below the MMP. For every scenario, the coefficient of variation was computed and oil recovery results were compared to a homogeneous reference model-designated as Model 1-which featured uniform horizontal and vertical permeabilities of 500 mD.

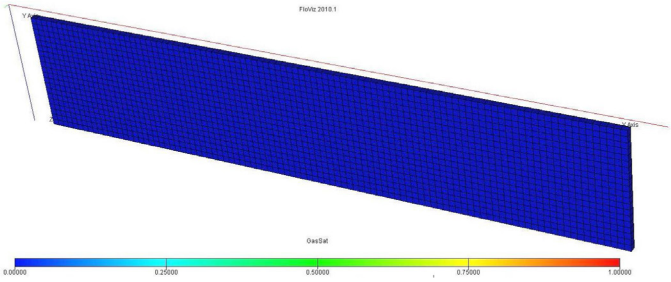

Figure 1: shows the initial gas saturation of the base case model (i.e., Model 1).

To assess the influence of anisotropy on CO_2 recovery, Models 2 through 4 were designed as homogeneous cases with varying kv/kh ratios. In these models, horizontal permeability was altered while vertical permeability remained fixed. Although the permeability values were uniform across all cells within each model, they varied between models. Notably, the kv/kh ratios in these three cases exceeded 1, which is relatively uncommon unless horizontal fissures or natural fractures are present. Conversely, Models 5 to 7 were developed to examine the impact of modifying vertical permeability while maintaining a constant horizontal permeability. It is important to highlight that in all six of these models, permeability values were consistent throughout each model but differed from one model to the next.

In a separate set of scenarios, Model 8 was designed with horizontal permeability increasing upward through the layers, while vertical permeability remained unchanged. Conversely, Model 9 featured vertical permeability that coarsened upward, with horizontal permeability held constant. In Model 10, both horizontal and vertical permeabilities were configured to coarsen upward simultaneously, resulting in isotropic conditions across each layer. To explore the impact of upward fining on CO_2-EOR performance, Models 11 through 13 were developed with grain sizes decreasing with height, leading to higher permeability at the base compared to the top of the model. Additionally, the influence of stratification on CO_2 recovery was examined by constructing models with alternating high and low permeability layers. For instance, Model 14 included layers of 500 mD and 100 mD, while Model 15 incorporated layers of 500 mD and 250 mD.

In an additional set of scenarios, Model 16 was configured with horizontal permeability randomly varying across layers, while vertical permeability remained unchanged. In contrast, Model 17 featured random variation in vertical permeability, with horizontal permeability held constant. The influence of diverse horizontal permeability values was further examined in Model 19, where these values were randomly assigned across layers, keeping vertical permeability fixed. Similarly, Model 20 utilized the same set of permeability values, but allowed variation in both horizontal and vertical directions. For Models 21 and 22, permeability was also randomly distributed among layers; however, each layer was isotropic, meaning horizontal and vertical permeabilities were equal. **(Table 1)** provides a summary of the permeability configurations used across all models in this study.

Table 1: Summarizes the permeability distributions of all cases in this study.

Model No.	**Horizontal Permeability Kh**	**Vertical permeability Kv**	**Kv/Kh ratio**	**Comments**
1	500	500	1	Homogeneous
2	125	500	4	Homogeneous
3	250	500	2	Homogeneous
4	375	500	1,333	Homogeneous
5	500	125	0,25	Homogeneous
6	500	250	0,5	Homogeneous
7	500	375	0,75	Homogeneous
8	coarsening upward	500		
9	500	coarsening upward		
10	coarsening upward	coarsening upward		
11	fining upwards	500		
12	500	fining upwards		
13	fining upwards	fining upwards		
14	alternating layers of 500 and 100 mD	alternating layers of 500 and 100 mD		
15	alternating layers of 500 and 250 mD	alternating layers of 500 and 250 mD		
16	Random	500		
17	500	random		
18	Random	500		
19	Random	random		Isotropic
20	Random	random		Isotropic
21	Random	random		Isotropic

Results and Discussion

Investigation of Minimum Miscibility Pressure (MMP)

The initial step involved determining the Minimum Miscibility Pressure (MMP) by running simulations for Models 2 through 14 under varying pressure conditions. Oil recovery was then plotted against pressure on a Cartesian scale after injecting 1.2 pore volumes (PV) over a 12-hour period. Models 2 to 4 were designed to assess the impact of reducing horizontal permeability relative to vertical permeability. As pressure increased, oil recovery improved until it stabilized around 175 bars, which was identified as the MMP. When these models were compared to the base case (Model 1), they exhibited a similar trend and the same MMP, indicating that a kv/kh ratio greater than 1 does not significantly influence recovery or MMP, as illustrated in **(Figure 2a)**. In contrast, Models 5 through 7 explored the effect of lowering vertical permeability while keeping horizontal permeability constant, resulting in kv/kh ratios below 1. These models also showed increasing recovery with pressure until it leveled off at approximately 175 bars, reaffirming the MMP, as shown in **(Figure 2b)**. Despite sharing the same MMP, the recovery rates varied among the models. A noticeable trend was that lower vertical permeability led to higher recovery. This is attributed to reduced vertical crossflow, which enhances horizontal displacement and improves sweep efficiency.

Additionally, Models 8 through 10 were designed to examine the impact of upward coarsening in horizontal permeability, vertical permeability and both simultaneously. Models 8 and 10 exhibited similar recovery trends with increasing pressure, identifying the Minimum Miscibility Pressure (MMP) within the range of 150 to 200 bars. These models also demonstrated lower recovery compared to Model 1 and Model 9, primarily because horizontal permeability was greater at the top of the reservoir than at the bottom. With vertical permeability held constant at 500 mD, increased crossflow redirected fluid into upper layers, causing oil bypass and early CO_2 breakthrough. In contrast, Model 9 achieved higher recovery than Models 8 and 10, as its vertical permeability increased upward while horizontal permeability remained fixed at 500 mD, as illustrated in **(Figure 2c)**. This configuration reduced vertical crossflow due to lower permeability at the base, promoting more effective horizontal displacement and improved sweep efficiency. Across all models, the MMP consistently fell between 150 and 200 bars and was ultimately determined to be 175 bars.

Additionally, Models 12 to 14 were used to examine the impact of upward fining in horizontal permeability, vertical permeability and both simultaneously. Upward fining refers to a permeability profile where values decrease from the bottom to the top of the model. In Model 12, oil recovery was notably high and closely matched that of the homogeneous base case. This is attributed to the lower vertical permeability at the top of the model, while horizontal permeability remained constant at 500 mD. As a result, vertical crossflow was minimized in the upper layers, allowing CO_2 to effectively sweep oil from those zones. Gravity also played a supportive role by promoting upward gas migration, enhancing sweep efficiency across most layers.

In contrast, Model 11, which featured only horizontal permeability fining upward and maintained vertical permeability at 500 mD, exhibited significantly lower recovery, as illustrated in **(Figure 2d)**. This is because vertical permeability is much higher than horizontal permeability and so cross flow occur and flow is diverted into lower layers only keeping the top layers unswept. The same occurs with Model 13 since both horizontal and vertical permeability are both fining so flow is diverted into lower layers with higher permeability.

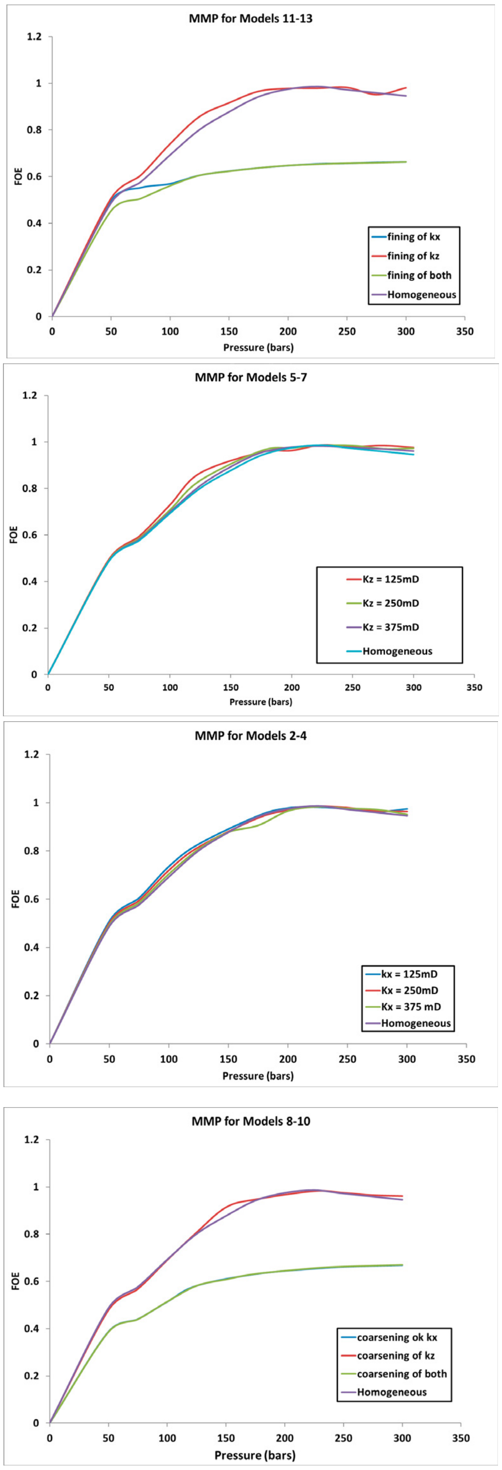

Figure 2: Shows the recovery versus pressure for a) Models 2-4, b) Models 5-8, c) Models 9-11 and d) Models 12-14.

Effect of heterogeneity on gas saturation

The following figures illustrate gas saturation in each model after six hours of CO_2 injection. Simulations were conducted at two pressure levels-100 bars and 250 bars-to observe behaviour before and after achieving miscibility. **(Figure 3)** presents the gas saturation profile for the homogeneous case (Model 1) at both pressure conditions. At 100 bars, where miscibility has not yet been reached, gas flow is primarily governed by gravity, causing the lighter CO_2 to rise and override the oil. As pressure increases to 250 bars, approaching the Minimum Miscibility Pressure (MMP), the extent of gas override diminishes, eventually forming a more uniform displacement front.

(Figure 4) displays the gas saturation in Model 3 after six hours of injection. Similar to the homogeneous case, gas movement below the MMP is dominated by gravity, with CO_2 rising due to its lower density relative to oil. However, once the MMP is attained, the fluids become miscible, their densities converge and the degree of gas override is significantly reduced.

Moreover, the extent of gas override diminishes as horizontal permeability is reduced. This occurs because, with a constant injection rate, lower horizontal permeability leads to increased pressure at the injector. As a result, the displacement becomes more miscible due to the elevated pressure and reduced permeability. When comparing Figure 4 to Figure 3, it is evident that gas fingering at the top of the model is absent, unlike in the homogeneous case and the gas distribution appears more uniform. A similar behaviour is observed in Models 2 and 4. **(Figure 5)** illustrates gas saturation in Model 6 at both pressure levels. Once again, the same trend is noted-at pressures below the MMP, gas rises due to its lower density, driven by gravity. As pressure increases, the degree of override gradually declines until a nearly uniform displacement front is established. It is also clear that decreasing vertical permeability reduces gas override, eventually resulting in a stable front, similar to scenarios with minimal crossflow.

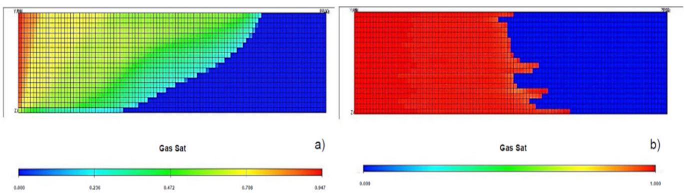

Figure 3: Shows gas saturation in Model 1 at a) 100 bars and b) 250 bars.

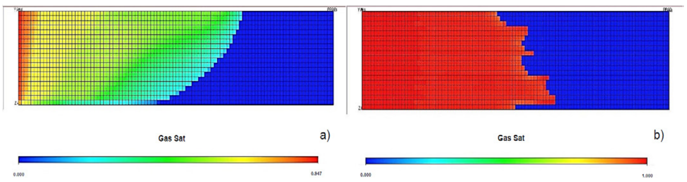

Figure 4: Shows gas saturation in Model 3 at a) 100 bars and b) 250 bars.

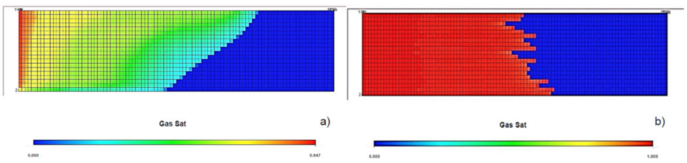

Figure 5: Shows gas saturation in Model 6 at a) 100 bars and b) 250 bars.

In Model 8, a significant degree of gas override is observed due to the natural tendency of gas to rise, driven by its lower density. This effect is further intensified by the high vertical permeability, which facilitates upward gas movement. As a result, the upper layers of the model exhibit nearly complete gas saturation, while the lower layers remain largely unswept. This behavior is consistent across all pressure levels but is more pronounced at pressures below the Minimum Miscibility Pressure (MMP). **(Figure 6)** illustrates the gas saturation distribution in Model 8 at 100 and 250 bars.

(Figure 7) presents the gas saturation for Model 10, where both horizontal and vertical permeabilities increase upward. Once again, gas override is evident, primarily due to the relatively low permeability at the base compared to the top layers. The low density of CO_2 contributes to its upward migration and this pattern persists across all pressures, with a stronger effect observed below the MMP.

(Figure 8) shows the gas saturation after six hours of injection in Model 12, which features upward fining of horizontal permeability-meaning the top layers have lower horizontal permeability than the bottom. This configuration causes the gas to slump downward. Although CO_2 naturally tends to rise, the limited horizontal permeability at the top restricts upward flow and the higher vertical permeability redirects the gas downward. At pressures below the MMP, gas saturation spans more layers due to gravity-driven flow attempting to override, but being hindered by low permeability at the top. At or above the MMP, the flow becomes viscosity-dominated, allowing gas to move efficiently through the more permeable lower layers.

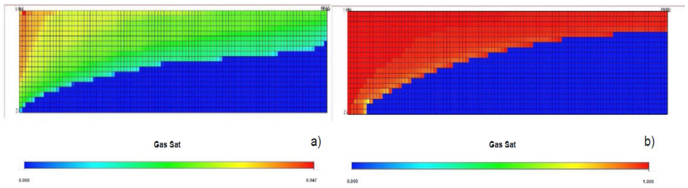

Figure 6: Shows gas saturation in Model 8 at a) 100 bars and b) 250 bars.

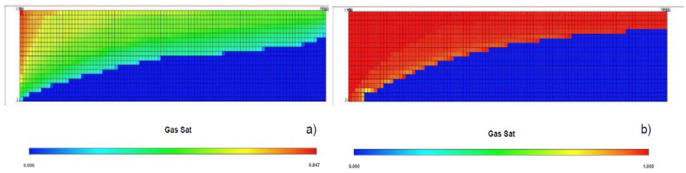

Figure 7: Shows gas saturation in Model 10 at a) 100 bars and b) 250 bars.

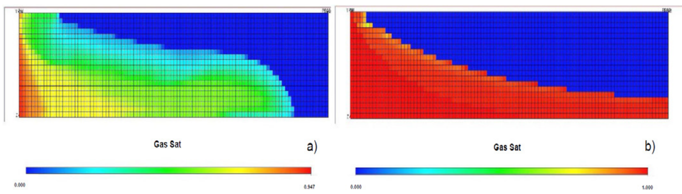

Figure 8: Shows gas saturation in Model 12 at a) 100 bars and b) 250 bars.

In Model 14, gas is observed to migrate downward due to the higher permeability at the bottom of the model compared to the top. **(Figure 9)** illustrates the gas saturation profile for Model 14, where both horizontal and vertical permeabilities decrease upward. At pressures below the Minimum Miscibility Pressure (MMP), gas saturation spans a wide portion of the model, driven by the natural tendency of gas to rise because of its lower density. However, at elevated pressures, the flow becomes less influenced by gravity and instead follows the path of higher permeability, moving more rapidly into the lower layers.

(Figure 10) presents the gas saturation in Model 15, which consists of uniform layers alternating between permeabilities of 500 mD and 100 mD. At pressures below the MMP, the stratification has minimal impact on the saturation profile and gas override dominates, with early breakthrough occurring in the upper layers. Once the MMP is reached, the flow becomes viscosity-driven and gas preferentially moves through the high-permeability layers, resulting in near-complete saturation in those zones and minimal saturation in the low-permeability layers-producing a fingering effect.

(Figure 11) shows the gas saturation in Model 16 at pressures below, at and above the MMP. Similar behavior to Model 15 is observed; however, the saturation in the lower-permeability layers is higher in Model 16 due to the smaller contrast in permeability values compared to Model 14.

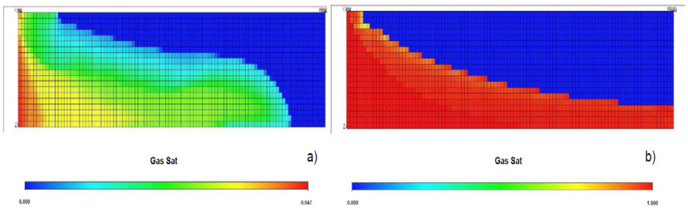

Figure 9: Shows gas saturation in Model 14 at a) 100 bars and b) 250 bars.

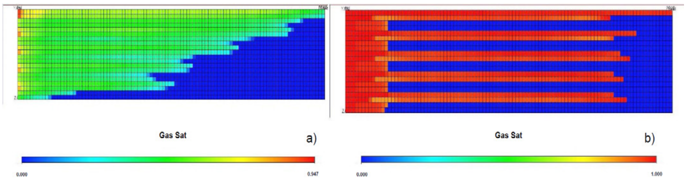

Figure 10: Shows gas saturation in Model 15 at a) 100 bars and b) 250 bars.

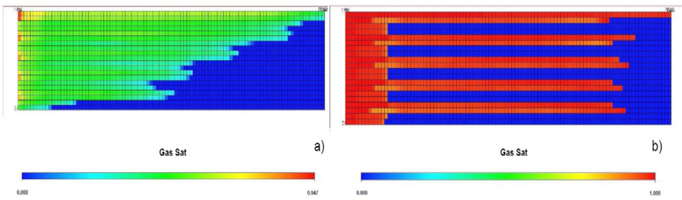

Figure 11: Shows gas saturation in Model 16 at a) 100 bars and b) 250 bars.

In Model 17, at a pressure of 100 bars, gas saturation extends across the entire model, exhibiting a near piston-like displacement. **(Figure 12)** illustrates the gas saturation profile for this model, where horizontal permeability is randomly assigned to each layer, while vertical permeability remains fixed at 500 mD. Due to the reduced horizontal permeability and constant vertical permeability, gas tends to rise because of its lower density but is restricted from spreading laterally. At the Minimum Miscibility Pressure (MMP), gas override is no longer observed and the flow becomes viscosity-dominated, favouring movement through high-permeability layers and bypassing others. This results in fingering and early breakthrough in those high-permeability zones.

(Figure 13) displays the gas saturation for Model 19, where horizontal permeability varies randomly with depth and vertical permeability is again held constant at 500 mD. At 100 bars, the flow is gravity-driven, with gas rising and overriding, leading to early breakthrough in the upper layers. As pressure increases, the override effect diminishes and gas preferentially flows through the more permeable layers, causing fingering and early breakthrough in those zones.

(Figure 14) presents the gas saturation for Model 20, which shares the same permeability values as Model 19, but allows variation in both horizontal and vertical directions. At lower pressures, gas override is less pronounced compared to Model 19, due to the presence of very low vertical permeability layers that inhibit crossflow. At MMP and above, the effect is the same as in Model 19 and the flow is viscous-dominated and moves through the high permeability layers faster.

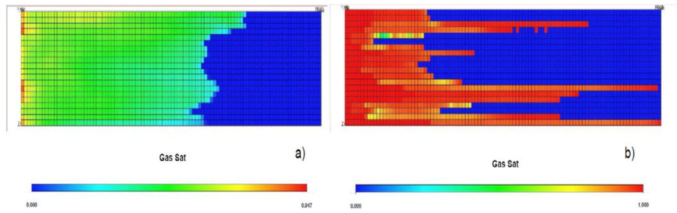

Figure 12: Shows gas saturation in Model 17 at a) 100 bars and b) 250 bars.

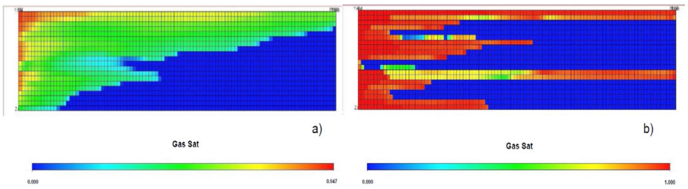

Figure 13: Shows gas saturation in Model 19 at a) 100 bars and b) 250 bars.

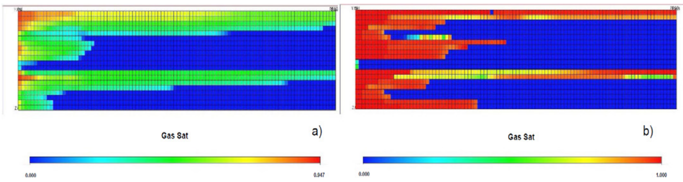

Figure 14: Shows gas saturation in Model 20 at a) 100 bars and b) 250 bars.

Effect of heterogeneity on oil recovery

It has become evident that reservoir heterogeneity and fine-scale geological features significantly influence gas saturation patterns, thereby impacting overall oil recovery. **(Table 2)** provides a summary of oil recovery results for each of the 22 models discussed earlier. Recovery values are recorded both before and at the Minimum Miscibility Pressure (MMP) following the injection of 1.2 pore volumes (PV) of CO_2. The improvement in recovery attributed to miscibility is also quantified. Additionally, the table includes the coefficient of variation for each scenario, serving as an indicator of the degree of heterogeneity present in the model.

It is evident that for the first eight models, oil recovery at the Minimum Miscibility Pressure (MMP) closely matches that of the homogeneous base case. Specifically, Models 2 to 4, which feature reduced horizontal permeability, yielded recovery rates comparable to the homogeneous model at MMP. In contrast, Models 5 to 7-where vertical permeability was decreased-exhibited a modest improvement in recovery, approximately 1-2% higher. These seven models have a coefficient of variation equal to zero, indicating uniform permeability across all layers. While the models are homogeneous in terms of permeability distribution, they differ in their kv/kh ratios, making them anisotropic. At pressures below the MMP, these models showed significantly lower recovery, with miscibility contributing to an approximate 22% increase in oil recovery.

It is observed that Model 9 achieves significantly higher oil recovery at the Minimum Miscibility Pressure (MMP) compared to Models 8 and 10. In Model 9, vertical permeability increases upward while horizontal permeability remains constant, resulting in reduced crossflow at the bottom and enhanced flow at the top, which contributes to improved recovery. In contrast, Models 8 and 10-where horizontal permeability was designed to coarsen upward-show notably lower recovery rates, around 63.1%. This indicates that upward coarsening of horizontal permeability has a pronounced negative impact on recovery. Below the MMP, all three models follow a similar trend, though overall recovery is lower. Model 9 exhibits a 25% improvement in recovery due to miscibility, while Models 8 and 10 show only an 11% increase.

Table 2: Summary of Cv and oil recovery for each model.

Model No.	Coefficient of variation (Cv)	Overall Oil Recovery (%) at MMP (175 bars)	Overall Oil Recovery (%) at 100 bars	Increase in oil Recovery due to miscibility (%)
1	0	94	69.2	24.8
2	0	94.6	73.6	21
3	0	93.6	72	21.6
4	0	94.4	70.4	24
5	0	95.6	72.8	22.8
6	0	96.2	70.7	25.5
7	0	95.4	69.9	25.5
8	0.44	63.1	51.4	11.7
9	0.44	94.7	69	25.7
10	0.44	63.1	51.4	11.7
11	0.44	63.6	56.9	6.7
12	0.44	96.5	74	22.5
13	0.44	63.8	56.1	7.7
14	0.56	84.5	51.6	32.9
15	0.28	70	55.2	14.8
16	0.54	76.3	59.3	17
17	0.54	95.7	59.6	36.1
18	0.79	70.7	56.6	14.1
19	0.79	61.5	47.2	14.3
20	0.65	65.5	59.2	6.3
21	0.34	77.6	68.4	9.2

Model 12 achieved a recovery of 96.5%, significantly higher than the 63.6% and 63.8% observed in Models 11 and 13, respectively. This enhanced performance is attributed to the upward fining of vertical permeability in Model 12, while horizontal permeability remained constant. In contrast, Model 11 featured upward fining of horizontal permeability with constant vertical permeability and Model 13 had both horizontal and vertical permeabilities fining upward. At a pressure of 100 bars, the same recovery pattern was observed, albeit with lower values. Additionally, Model 12 showed a 22% improvement in recovery due to miscibility, whereas Models 11 and 13 exhibited only a 7% increase.

Models 14 and 15 consist of alternating layers with high and low permeability. Model 14 achieved an oil recovery of 84.5%, whereas Model 15 reached only 70%. This difference is attributed to the greater contrast in permeability in Model 14, which features layers of 500 mD and 100 mD, compared to Model 15's layers of 500 mD and 250 mD. Consequently, Model 14 has a coefficient of variation (Cv) of 0.56, while Model 15 has a lower Cv of 0.28. The higher recovery in Model 14 is due to the isotropic nature of the layers—where vertical and horizontal permeabilities are equal-resulting in reduced vertical flow and limited gas crossflow, thereby enhancing horizontal sweep efficiency. Additionally, Model 14 shows a greater improvement in recovery due to miscibility (32.9%) compared to Model 15, which exhibits only a 14.8% increase.

Models 16 and 17 were designed with randomly distributed permeability-Model 16 in the horizontal direction and Model 17 in the vertical. Model 16 yielded a significantly lower oil recovery of 76.3%, whereas Model 17 achieved a much higher recovery of 95.7%. This outcome highlights that altering horizontal permeability while keeping vertical permeability constant leads to reduced recovery, as it promotes greater gas override. Consequently, more oil is bypassed, resulting in lower efficiency. This trend is consistent at pressures below the Minimum Miscibility Pressure (MMP) as well.

Model 18 achieved an oil recovery of 70.5%, notably higher than the 61.7% recorded for Model 19. Both models explored the impact of randomly distributed permeability; however, Model 18 featured random variation in horizontal permeability while maintaining a constant vertical permeability. In contrast, Model 19 had randomness in both horizontal and vertical directions, which contributed to its lower recovery. Despite the differences in configuration, both models experienced a similar improvement in recovery due to miscibility, with an increase of approximately 14%.

Models 20 and 21 exhibit different recovery outcomes—65.5% and 77.6%, respectively—despite both having randomly distributed permeability in both horizontal and vertical directions. The variation in recovery is attributed to the difference in their coefficient of variation (Cv), with Model 20 having a Cv of 0.65 and Model 21 a lower Cv of 0.34. Since Model 21 is more homogeneous, it achieves better recovery performance. However, the improvement in recovery due to miscibility is relatively modest for both cases, with Model 20 showing a 6.3% increase and Model 21 a 9.2% increase.

Effect of coefficient of variation on recovery

To explore whether a correlation exists between the coefficient of variation (Cv) and oil recovery, a comparative analysis is conducted across the different models. For meaningful comparison, the models are categorized based on the direction in which permeability varies. This section evaluates the impact of modifying horizontal permeability alone, vertical permeability alone and both simultaneously. As an illustration, **(Table 3)** presents the recovery values at 175 bars along with the corresponding Cv for models where horizontal permeability was varied while vertical permeability remained constant at 500 mD.

Table 3: Oil recovery for variation in horizontal permeability.

Model	Cv	Oil Recovery
8	0.44	63.1
11	0.44	63.6
16	0.54	76.3
18	0.79	70.7

Moreover, **(Table 4)**. shows the recovery and Cv for the models in which vertical permeability was made to vary and horizontal permeability was made constant at 500mD.

Table 4: Oil recovery for variation in vertical permeability.

Model	Cv	Oil Recovery
10	0.44	94.7
13	0.44	96.5
18	0.54	95.7

Furthermore, **(Table 5)**. shows the recovery and Cv for the models in which both the horizontal and vertical permeability was made to vary simultaneously.

Table 5: Oil recovery for variation in both kx and kz

Model	Cv	Oil Recovery
11	0.44	63.1
14	0.44	63.8
15	0.56	84.5
16	0.28	70
20	0.79	61.5
21	0.65	65.5
22	0.34	77.6

Conclusions

Knowing what happens to the flow of CO_2 and hydrocarbon in the presence of fine-scale geological structures is important to determine the amount of CO_2 needed and how much hydrocarbon will be recovered. Understanding whether the flow is viscous-dominated or gravity-dominated could give some economic indications on the project and prevent the bypass of valuable oil. After running 21 models and analyzing the different outputs, the following were concluded:

- The MMP for all models was found to be between 150 bars and 200 bars and was taken to be 175 bars. At pressures below the MMP, flow tends to be gravity-dominated and is affected mostly by gravity and less by permeability and tends to override. At pressures higher than the MMP, the oil and gas become one phase and the flow is viscous-dominated and takes the path of least resistance or highest permeability first. As a result, fingering occurs and early breakthroughs occur in these layers.
- All models show an increase in recovery due to miscibility. Having a kv/kh ratio greater than unity does not affect oil recovery and yields a similar recovery as that of the homogeneous. On the other hand, having kv/kh ratio less than unity affects oil recovery. As the ratio decreases, the recovery increases, with the best recovery being at kv=0 (i.e., no cross flow).
- Coarsening of the vertical permeability only does not have significant effect on oil recovery but the coarsening of the horizontal or both horizontal and vertical permeabilities reduces recovery greatly. Also, fining of vertical permeability does not affect oil recovery but fining of either horizontal permeability or both reduces recovery by a great amount.
- The degree of gas override increases or decreases depending on both horizontal and vertical permeability. For example, having random permeability distribution distorts the flood front and causes fingering and the effect of gas override diminishes.
- The variation of horizontal permeability has the most effect on oil recovery, regardless of whether vertical permeability is constant or varying as well. However, the coefficient of variation cannot be used alone as a measure of heterogeneity in CO_2 flooding, since two models with the same Cv value can yield different recoveries. No relation between Cv and recovery could be determined from the current available data.

References

1. Bello A, Ivanova AA, Cheremisin A. A Comprehensive Review of the Role of CO2 Foam EOR in the Reduction of Carbon Footprint in the Petroleum Industry. Energies 2023;16(3):1167.
2. Ganzer L, Ganzer L, Reinicke KM, et al. Enhanced Oil Recovery 2017:1-57.
3. Deng X, Deng X, Tariq Z, et al. Relative Contribution of Wettability Alteration and Interfacial Tension Reduction in EOR: A Critical Review. J Molecular Liquids 2020;325:115175.
4. Iravani M, Khalilnezhad Z, Khalilnezhad A. A Review on Application of Nanoparticles for EOR Purposes: History and Current Challenges. J Petro Exploration Production Tech 2023;13(4):959-994.
5. Vladimir A, Manrique E. Enhanced Oil Recovery: Field Planning and Development Strategies. Gulf Professional Publishing 2010.
6. Ahmed R, Mansour EM. Enhanced Oil Recovery: Chemical Flooding. Geophysics and Ocean Waves Studies 2021;51.
7. Shah R, Batrisyia Bt N, Bt Sazali RA, et al. Nanomaterials for Scaling Prevention in Alkaline–Surfactant–Polymer Flooding: A Review. Applied Nanoscience 202313(6):3945-3974.
8. Farzad P, Zargar G, Kadkhodaie A, et al. Experimental Evaluation of Designed and Synthesized Alkaline-Surfactant-Polymer (ASP) for Chemical Flooding in Carbonate Reservoirs. Fuel 2022;321:124090.

9. Juan DA, Miri R, et al. In Situ Combustion: A Comprehensive Review of the Current State of Knowledge. Energies 2023;16(17):6306.

10. Yi P, Qiao W, Chi D, et al. Research of Steam Injection In-Situ Production Technology to Enhance Unconventional Oil and Gas Recovery: A Review. J Analytical and Applied Pyrolysis 2023:106332.

11. Fang Z, Xi C, Zhang X, et al. Analysis on the Main Influential Factors of Post-Steam In-Situ Combustion Performance in Heavy Oil Reservoir. J Japan Petro Institute 2021;64(2):76-83.

12. Fang Z, Xi C, Zhang X, et al. Evaluation of a Field-Wide Post-Steam In-Situ Combustion Performance in a Heavy Oil Reservoir in China. In SPE Russian Petroleum Technology Conference. OnePetro 2020.

13. Aurel C. Applied Enhanced Oil Recovery 1992.

14. Syed FI, Syed FI, Muther T, et al. CO2 EOR Performance Evaluation in an Unconventional Reservoir through Mechanistic Constrained Proxy Modeling. Fuel 2022;310:122390.

15. Xu Z, Zhengxiao X, Huang G, et al. A Review of Development Methods and EOR Technologies for Carbonate Reservoirs. Petro Sci 2020;17(4):990-1013.

16. Lu J, Hawthorne S, Sorensen J, et al. Advancing CO2 Enhanced Oil Recovery and Storage in Unconventional Oil Play-Experimental Studies on Bakken Shales. Applied Energy 2017;208:171-183.

17. Isah A, Isah A, Arif M, et al. A Systematic Review of Anhydrite-Bearing Reservoirs: EOR Perspective, CO2-Geo-Storage and Future Research. Fuel 2022;320:123942-123942.

18. Pimenta G, Pimenta G, Romero C, Romero C. CO2 EOR Challenges and Opportunities to Enable CCUS Strategies 2022.

19. Alklih MY, Alklih MY, Aljneibi NM, et al. Does Miscibility Alone Predict the Success of WAG Projects? Key Issues in Miscible HC-WAG Injection 2021.

20. Tarek A. Reservoir Engineering Handbook. United States of America: Elsevier Inc 2006;1.

21. Alshuaibi M, Alshuaibi M, Farzaneh SA, et al. An Experimental and Simulation Investigation on the Effect of Different Gas Mixtures on Performance of Miscible CO2 Injection in HPHT Abu Dhabi Reservoir 2018.

22. Alklih MY, Alklih MY, Al Hammadi KE, et al. First CO2-EOR Project of the Middle East, Lessons Learnt and Future Plan after Two Years of Injection 2019.

23. Talebian SH, Talebian SH, Masoudi R, et al. Foam Assisted CO2-EOR: A Review of Concept, Challenges and Future Prospects. J Petro Sci Eng 2014;120:202-215.

24. Holm LW, Josendal VA. Mechanisms of Oil Displacement by Carbon Dioxide. J Petro Tech 1974;26(12):1427-1438.

Appendix A

Table A.1: Component Fluid Properties.

Component	Critical Temperature (K)	Critical Pressure (bars)	Acentric Factor	Molecular Weights	Boiling Points (K)	Initial oil Composition
CO2	304.2	72.80	0.225	44.010	194.7	0.0118
N2-CH4	189.67	45.24	0.0084	16.208	113.656	0.1170
C2-NC4	338.44	41.92	0.1481	44.793	259.432	0.1945
IC5-C7	556.92	31.31	0.2485	83.458	340.618	0.2202
C8-C12	667.51	23.86	0.3279	120.524	415.671	0.2815
C13-C19	769.00	17.23	0.5672	210.743	543.642	0.0940
C20-C30	801.51	11.9	0.9422	401.926	735.01	0.0809

Table A.2: Reservoir Properties.

Parameter	Value	Units
Porosity	0.1	-
Permeability in the x-direction	500	mD
Permeability in the z-direction	500	mD
Rock Compressibility	5x10-5	Bars-1
Temperature	53	C
Capillary Pressure	0	Bars
Wellbore Diameter	0.02	m
CO2 injection rate	0.48	m3/day

Table A.3: Relative permeability data

Sg	Krg	Krog	Pc
0	0	1	0
0.02	0	1	0
0.045	9.21E-05	0.8538	0
00.07	0.000642	0.7233	0
0.095	0.002	0.6076	0
0.12	0.0045	0.5056	0
0.145	0.0084	0.4164	0
0.17	0.0139	0.3388	0
0.195	0.0214	0.2721	0
0.22	0.0312	0.2152	0
0.245	0.0433	0.1673	0
0.27	0.0582	0.1275	0
0.295	0.076	0.0948	0
0.32	0.097	0.0686	0
0.345	0.1214	0.048	0
0.37	0.1494	0.0321	0
0.395	0.1813	0.0204	0
0.42	0.2172	0.0121	0
0.445	0.2574	0.0065	0
0.47	0.302	3.05E-03	0
0.495	0.3514	1.15E-03	0
0.52	0.4057	2.89E-04	0
0.545	0.4651	0	0
0.57	0.5298	0	0
0.595	0.6001	0	0
0.62	0.6761	0	0
0.645	0.758	0	0
0.67	0.846	0	0
0.71	1	0	0
0.77	1	0	0
0.83	1	0	0

Table A.4: Permeability distribution for models 2-4.

Model no.	Horizontal permeability (mD)	Vertical permeability (mD)	Kv/kh ratio
2	125	500	4
3	250	500	2
4	375	500	1.333
5	500	300	
6	500	250	
7	500	200	
8	500	150	
9	500	100	
10	350	50	

Table A.5: Permeability distribution for models 5-7.

Model no.	Horizontal permeability (mD)	Vertical permeability (mD)	K v / k h ratio
5	500	125	0.25
6	500	250	0.5
7	500	375	0.75

Table A.6: Permeability distribution for model 8.

Layer no.	Horizontal Permeability (mD)	Vertical Permeability (mD)
1	500	500
2	450	500
3	400	500
4	350	500
5	300	500
6	250	500
7	200	500
8	150	500
9	100	500
10	50	500

Table A.7: Permeability distribution for model 9.

Layer no.	Horizontal Permeability (mD)	Vertical Permeability (mD)
1	500	500
2	500	500
3	40	500
4	350	500

Table A.8: Permeability distribution for model 10.

Layer no.	Horizontal Permeability (mD)	Vertical Permeability (mD)
1	500	500
2	450	450
3	400	400
4	350	350
5	300	300
6	250	250
7	200	200
8	150	150
9	100	100
10	50	50

Table A.9: Permeability distribution for model 11.

Layer no.	Horizontal Permeability (mD)	Vertical Permeability (mD)
1	50	500
2	100	500
3	150	500
4	200	500
5	250	500
6	300	500
7	350	500
8	400	500
9	450	500
10	500	500

Table A.10: Permeability distribution for model 12.

Layer no.	Horizontal Permeability (mD)	Vertical Permeability (mD)
1	500	50
2	500	100
3	500	150
4	500	200
5	500	250
6	500	300
7	500	350
8	500	400
9	500	450
10	500	500

Table A.11: Permeability distribution for model 13.

Layer no.	Horizontal Permeability (mD)	Vertical Permeability (mD)
1	50	50
2	100	100
3	150	150
4	200	200
5	250	250
6	300	300
7	350	350
8	400	400
9	450	450
10	500	500

Table A.12: Permeability distribution for model 14.

Layer no.	Horizontal Permeability (mD)	Vertical Permeability (mD)
1	500	500
2	100	100
3	500	500
4	100	100
5	500	500
6	100	100
7	500	500
8	100	100
9	500	500
10	100	100

Table A.13: Permeability distribution for model 15.

Layer no.	Horizontal Permeability (mD)	Vertical Permeability (mD)
1	500	500
2	250	250
3	500	500
4	250	250
5	500	500
6	250	250
7	500	500
8	250	250
9	500	500
10	250	250

Table A.14: Permeability distribution for model 16.

Layer no.	Horizontal Permeability (mD)	Vertical Permeability (mD)
1	150	500
2	300	500
3	50	500
4	200	500
5	100	500
6	200	500
7	400	500
8	250	500
9	50	500
10	500	500

Table A.15: Permeability distribution for model 17.

Layer no.	Horizontal Permeability (mD)	Vertical Permeability (mD)
1	500	150
2	500	300
3	500	50
4	500	200
5	500	100
6	500	200
7	500	400
8	500	250
9	500	50
10	500	500

Table A.16: Permeability distribution for model 18. .

Layer no.	Horizontal Permeability (mD)	Vertical Permeability (mD)
1	500	500
2	200	500
3	65	500
4	250	500
5	180	500
6	10	500
7	800	500
8	150	500
9	60	500
10	200	500

Table A.17: Permeability distribution for model 19.

Layer no.	Horizontal Permeability (mD)	Vertical Permeability (mD)
1	500	500
2	200	200
3	65	65
4	250	250
5	180	180
6	10	10
7	800	800
8	150	150
9	60	60
10	200	200

Table A.18: Permeability distribution for model 20.

Layer no.	Horizontal Permeability (mD)	Vertical Permeability (mD)
1	46	46
2	656	656
3	200	200
4	365	365
5	789	789
6	365	365
7	62	62
8	200	200
9	652	652
10	50	50

Table A.19: Permeability distribution for model 21.

Layer no.	Horizontal Permeability (mD)	Vertical Permeability (mD)
1	250	250
2	220	220
3	500	500
4	320	320
5	700	700
6	400	400
7	200	200
8	300	300
9	500	500
10	600	600